International Journal of Engineering

Journal Homepage: www.ije.ir

NiO-Ni-Al_2O_3(γ) Nanocatalyst by Pulse Electrocodeposition Over Ni Open-cell Foam for Methane Reforming

M. Zafardoagoo*[a], S. K. Sadrnezhaad[b], J. Mostaghimi[c]

[a] *Department of Materials Science and Nanotechnology, School of Science and Engineering, Sharif University of Technology, International Campus-Kish Island, Iran*
[b] *Department of Materials Science and Engineering, Sharif University of Technology, Azadi Ave., Tehran, Iran*
[c] *Centre for Advanced Coating Technologies, Faculty of Applied Science & Engineering, University of Toronto, 5 King's College Road, Toronto, Ontario, M5S 3G8, Canada*

PAPER INFO

Paper history:
Received 16 June 2023
Received in revised form 24 July 2023
Accepted 26 July 2023

Keywords:
Nickel Foam
γ-alumina
Methane Reforming
Nanocatalyst
Pulse Electrocodeposition

ABSTRACT

Global warming persuades researchers to improve the effectiveness of renewable energy technologies, such as H_2 production by methane steam reforming (MSR) an endothermic process. Herein, a nanocatalyst based on open-cell nickel foam 40 (pore per inch) with high thermal conductivity was prepared. The nanocatalyst was synthesized with a chemical stepwise synthesis approach, chemical pre-treatment, pulsed electrocodeposition of Ni-Al_2O_3(γ) nanoparticles, and calcination. Measurements of thermal diffusivity(α) with flash xenon technique gained 4.41×10^{-6} m^2s^{-1} and values of specific heat capacity, Cp, by differential scanning calorimetry (DSC) and thermal conductivity(λ) enhanced by 65% in temperature range of 150 to 550°C in Ni-alumina(γ) foam nanocatalyst. Furthermore, characterization and tests for comparing nickel foam and Ni-alumina(γ) foam indicated that the hardness improved from 145 Vickers hardness (HV) to 547 HV and compression strength increased from 1.1 MPa to 5MPa and specific surface area (S_{BET}) from 1.48 m^2g^{-1} to 48 m^2g^{-1}. XRD (x-ray diffraction) analysis showed NiO and $NiAl_2O_4$ in the structure. The interface between the catalytic component ($NiAl_2O_4$), and nickel affected the catalytic ability for MSR, and the efficiency gained at low tempreture 500 °C was the same as reported at 720°C by other investigations.

***doi**: 10.5829/ije.2023.36.10a.15*

Graphical Abstract

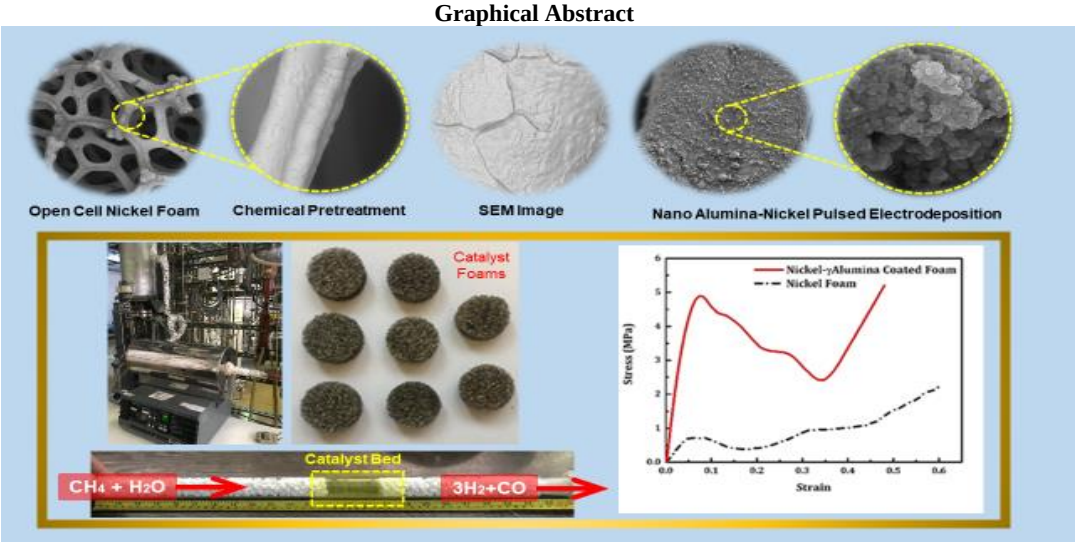

*Corresponding Author Email: m.zafardoago@gmail.com (M. Zafardoagoo)

Please cite this article as: M. Zafardoagoo, S. K. Sadrnezhaad, J. Mostaghimi, NiO-Ni-Al_2O_3(γ) Nanocatalyst by Pulse Electrocodeposition Over Ni Open-cell Foam for Methane Reforming, ***International Journal of Engineering, Transactions A: Basics***, Vol. 36, No. 10, (2023), 1908-1918

NOMENCLATURE

Cp	Specific thermal capacity($Jg^{-1}{}_{\circ}C^{-1}$)	**Greek Symbols**	
HV	Vickers hardness	ρ	Density (kg/m^3)
MPa	Mega Pascal	α	Thermal diffusivity(m^2S^{-1})
MSR	Methane Steam Reforming	λ	Thermal conductivity ($Wm^{-1}{}_{\circ}C^{-1}$)
PPI	Pore per Inch	θ	Duty cycle (%)
f	Frequency (Hertz)		

1. INTRODUCTION

Environmental concerns of fossil fuels have motivated scientists to develop sustainable energies like wind, solar and hydrogen. Hydrogen is a clean energy with no exhaust contaminants during combustion [1]. The availability of immense natural gas reservoirs in the globe justifies reforming natural gas methane, to produce hydrogen by steam, carbon dioxide, and oxygen. The endothermic methane steam reforming, MSR, reaction Equation (1) required extensive energy at a temperature range of 700-720 °C on the catalytic bed.

$$CH_4 + H_2O \rightarrow CO + 3H_2 \qquad \Delta H^{\circ}_{298} = +206 \ \frac{kJ}{mol} \qquad (1)$$

Mostly water gas shift reaction (WGS) Equation (2) goes along MSR.

$$CO + H_2O \rightarrow CO_2 + H_2 \quad \Delta H^{\circ}_{298} = -41.1 \frac{kJ}{mol} \qquad (2)$$

Moreover, during MSR some side reactions occur at high temperatures (T > 750 °C) via Equation (3), and Boudouard reaction at low temperatures (300–450 °C) as Equation (4) [2].

$$CH_4 \rightarrow C_{(s)} + 2H_2 \qquad \Delta H^{\circ}_{298}=+75.6 \frac{kJ}{mol} \qquad (3)$$

$$2CO \rightarrow C_{(s)} + CO_2 \qquad \Delta H^{\circ}_{298}=-172 \ \frac{kJ}{mol} \qquad (4)$$

Usually, combining transition and/or noble metals catalysts on stabilized supports (alumina, ceria, ceria promoted alumina, zeolite, etc. in catalysts have been frequently used [3-5]. However, nickel was the most common catalyst for being cheap, active, and selective in MSR [6, 7]. Nevertheless, considering some drawbacks like Ni-sintering and carbon deposition maybe by hotspots and poor uniform temperature profile of pelletized catalysts bed, persuade researchers to modify catalysts structure [8-12]. Therefore, any attempt to fabricate novel catalysts for lowering carbon deposition, good heat transfer, decrease energy consumption, high thermal stability, high mechanical strength and increase lifetime are valuable [13-15]. Open-cell metal foams have a special set of materials properties such as low density, high thermal conductivity, ductility, resilience to thermal shock resistance, fluid permeability, and high surface area [16, 17]. Recently, application of nickel foams in MSR have been investigated for good heat distribution which increased [18] the CH_4 conversion inside the reformers by high interface area between the gaseous reactants and the microporous catalysts [19-21]. In fact, higher thermal conductivity limits the thermal gradient among reactants to gain higher catalytic performance in methane reforming [9, 10, 15, 22-24]. Moreover, metal foams are attractive for compression loading applications such as in catalysts bed for their progressive crushing whilst tensile loading caused a fast, brittle fracture [16]. In the compression stress-strain curve of metallic foams three deformation stages seen as 1. Linear short elastic, 2. Long plastic plateau and 3. Densification [25-30]. Thus, this study place a focus on developing nickel foam structured catalyst reinforced by alumina (γ) nanoparticles to increase the plastic plateau region for mechanical strengthening and prevent catalyst brittle crushing [23, 31].

Furthermore, recently it is studied to find that catalytic performance of the Ni foam based catalyst is highly dependent on the pre-treatment and reaction temperature [18, 32, 33]. Pegios et al. [34] reported a Ni-foam catalyst aluminium oxide precursors by dip coating method over Ni-foams with MgO and SiO_2 as promoters for methane reforming. Results indicated that chemical pretretment conditions increase the active metal surface and active sites probably at the nickel-alumina interface.

Chai et al.[33] indicated among Ni/MO_x(M=Al, Zr or Y) binary catalysts, Ni foam/ Al_2O_3 possesses the largest specific surface area and the highest amount of NiO species (Ni active site), and as a result, exhibits the best catalytic performance. Lajevardi et al. [35] indicated that Ni-nano Al_2O_3 with applied pulse electrcodeposition had higher hardness than direct current. Applied nano-particles locked dislocation at the grain boundaries movements and recrystallization at elevated temperatures. Therefore, microhardness and thermal stability increased [36-38]. In the pulse current state, less nano particles agglomerated, and caused more uniform dispersion of nano particles [39]. The metal foam structure does not in itself have a high surface area; thus, in catalyst applications, deposition of a high surface area coat e.g., $Al_2O_3(\gamma)$, SiO_2, or zeolite by wash-coating, sol-gel, electrochemical deposition, electrophoretic, chemical vapor deposition (CVD) or physical vapor deposition (PVD) is necessary [9, 40, 41].

The utilization of appropriate ceramic nanoparticles with high specific surface area such as $Al_2O_3(\gamma)$ reinforcement in a porous metal matrix in catalysis would be interesting candidate for enhancing thermal conductivity, hardness and compression strength [17, 42-

44]. Cimino et al. [18] applied Re/Ce via electroprecipitation and pulse deposition methods on nickel foam catalyst in methane reforming to increase heat transfer by support metal foam strucure. To date, only a limited number of studies have been examined the effect of alumina(γ) nanoparticles in Ni-foam as nanocatalyst by pulse codeposition for compression strengthening, more thermal conductivity and MSR operating at low temperature as a way of energy saving. By applying this concept, we aim at increased thermal conductivity, a lower thermal gradient through the reaction chamber for more heat transfer and better interaction between the gas-solid reactantants'active Ni phase and alumina(γ) nanoparticles. The MSR pilot test of this nanocatlyst indicated the same efficiency at 500 °C compared to MSR efficiency of common catalysts at 720 °C that reported by other works [9, 22, 23].

2. MATERIALS METHOD

2. 1. Experimental The procedure consists of several steps for nanocatalyst fabrication of nickel-alumina(γ) foam, briefly, such as (a) open-cell nickel foam fabrication over polyurethane (PU) as substrate, (b) chemical pre-treatment or etching, and (c) Ni-alumina(γ) nanoparticles pulse electro co-deposition. Firstly, the 40 pores per inch (ppi) open cell PU with the density of 0.021 gcm^{-3} became conductive by nickel electroless deposition. We used the electroless bath containing nickel sulfate and sodium hypo-phosphide ($NaPO_2H_2$) at 82-85ºC with a pH of 4. Afterward, the foam was nickel electrodeposited by complex nickel salt solution (including nickel(II) sulfate hexahydrate ($NiSO_4.6H_2O$), Merck 180 gL^{-1}, ammonium chloride (NH_4Cl), Merck 25 gL^{-1} and boric acid (H_3BO_3), Merck, 30gL^{-1}) at 55 ºC, pH 5.5, and direct surface current density 20 Adm^{-2} for 60 min. All the chemicals used with the grade for analysis. Then foam was put into a tube furnace flowing 99.99% purity argon gas to eliminate the PU substrate by pyrolysis as per the procedure explained in another work [16]. In continue, chemical pre-treatments were applied to increase the roughness of the surface of the foam's strands in 6 Molar (M) hydrochloric acid (HCl) at three different temperatures (i.e., 60, 70, and 80 ˚C) for 10 and 15 minutes. Then the foam was rinsed thoroughly with deionized water, dipped into acetone and dried. Each specimen with dimensions 10×40×40 mm^3 was pulse electro codeposited by two solutions to gain nickel-γ-alumina nanocomposite over the etched nickel foam. Analytical reagents and deionized water were used to prepare the plating solutions. Firstly, a suspension of nano Al_2O_3(γ) powder (99.99%, particle size 20-50 nm, BET surface area >150 m^2g^{-1}) (5 gL^{-1}) and sodium dodecyl sulfate (SDS) (1.5 gL^{-1}) as surfactant dispersed, stirred for 21 hours with 200 rpm and agitated by ultrasonic waves for 20 min to break the weak-bonded agglomerations. Secondly, the nickel watt bath type (including nickel(II) sulfate hexahydrate ($NiSO_4.6H_2O$), Merck, 250 gL^{-1}, Nickel(II) chloride - hexahydrate ($NiCl_2.6H_2O$) 40 gL^{-1}, boric acid (H_3BO_3), 35 gL^{-1}) was prepared. Then the nano-suspension was added to it and well stirred. Afterwards, pulsed electro co-deposition was performed with frequency 5 Hz, duty cycle 50%, current density 27.5 Adm^{-2}, stirring rate 200 rpm, the electrolyte pH 4.2, temperature 50±2ºC exposed time 90 minutes for nickel foam as the cathode. Finally, the pulse electrodeposited nickel-nano γalumina foam was rinsed with deionized water, dried, and calcined at 720 ºC.

2. 2. Characterization and Tests We performed the thermogravimetric analysis (TG, TA Instrument BAHR STA 503) to determine the thermal stability of the PU foam before plating. In this study, X-ray diffraction (XRD) patterns for identifying crystalline phases of the specimens were collected with a PANalytical X-ray diffractometer using Cu K_α radiation (λ=0.15406 nm, 40 kV, 40 mA). Scanning electron microscopy (SEM) and field emission electron microscopy (FESEM) were used to investigate the specimen morphology and elemental analysis. The compression strength test of the specimens with dimensions 10×20×20 mm^3 was conducted at room temperature by HOUNSFIELD (H10KS-UK) test machine. The surface hardness (on the Vickers scale) of nanocomposite coatings was measured by a micro-hardness measurement device that applied a 50 g load for 15 seconds. The nickel foam specimens were etched for 15 s with a mixture of 3 mL HF and 80 mL HNO_3, and the thickness of struts was determined by an optical microscope. Specific heat capacity Cp was measured by the Mettler Toledo thermal analysis with N_2 gas flow and thermal diffusivity α by Xenon Flash model XFA 500 was quantified. The H_2-TPR (temperature-programmed reduction) experiments were carried out in the NanoSord instrument (Sens Iran Co.), under a mixture of 5% H_2-95% argon gas with 10 sccm flow rate to determine the reducibility of nickel-alumina catalyst. Ni-alumina(γ) foam specimen was heated with a rate of 10 º $Cmin^{-1}$ up to 950 º C.

2. 3. Experimental Set-Up for Catalytic Reaction The performance of the foam catalysts was studied in a pilot system under atmospheric pressure, as shown in Figure 1. A quartz tube reactor with a 28 mm inner diameter was loaded with a 7.64 g synthesized foam catalyst, 50 mL, and the remained volume was filled with inactive alumina(α). First, the Ni-alumina(γ) foam was reduced in situ before injecting methane/steam mixture by pure hydrogen at 430 ºC for 120 min with a 5 º$Cmin^{-1}$ heating rate. The methane-water mixture (Steam/CH_4; v/v:3) was injected into the quartz tube through a dosing

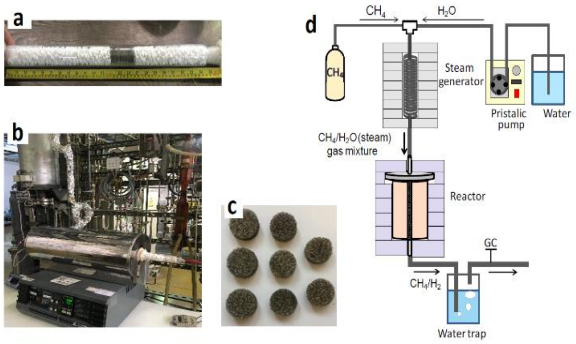

Figure 1. (a) Quartz tube filled with Ni-alumina foam catalysts, (b) catalysts of test pilot, (a) Ni- alumina (γ) foams, and (d) schematic picture for catalyst test setup

pump (LATEK- P700), which controlled the feed rate with gas hourly space velocity (GHSV) of 2000 h^{-1}. The tube reactor temperature was set at 500 ºC. The product gasstream passed through a condenser at the outlet of the reactor, and the unreacted water was stored in a tank. The dry gas outlet (H_2, CH_4) was analyzed by the online gas chromatography (GC) (model Agilent Technologies 6890N) equipped with a thermal conductive detector (TCD) and flame ionization detector (FID). The catalytic performances of the Ni-alumina(γ) coated layer on nickel foam prepared in situ were measured.

3. RESULTS AND DISCUSSION

Thermogravimetric analysis was performed to determine the thermal stability of polyurethane foam by using a TA Instrument BAHR STA 503. Samples of 0.22g were heated up to 650 ºC at a heating rate of 10 ºCmin^{-1} in a nitrogen atmosphere. As shown in graph Figure 2, a very slight rate change seen at 100-120 ºC may be for water evaporation while PU foam was decomposing with a rapid rate at 290-400 ºC that was associated with the polyol main chain and urethane bond breaking as reported by other researches [45, 46]. As mentioned pyrolysis was done to remove PU substrate with the least probable crack formation by a controlled procedure [16]. Moreover, the alumina must penetrate uniformly inside the tortuous nickel foam without blocking the foam pores. In continue chemical pre-treatment by 6 M HCl was applied to the pure nickel foam to increment the adhesion of the strands' surface for pulsed electrodeposition of Ni-γalumina [34]. As per SEM images, in Figure 3(a), pure nickel foam showed sound struts with no cracks. Moreover, in Figure 3(b), (c) and (d) grain boundaries of nickel foams pre-treated in HCl at 70 and 80 ºC for 10 and 15 minutes were obviously seen. Here, the foam at 70 ºC in HCl was observed more stable than that of the specimen heated at 80 ºC, however, etching the foam at severe conditions, heated at 80 ºC for 15 min, caused the foam losing integrity. Therefore, the optimized condition for chemical pretreatment by 6 M HCl at 80 ºC for 10 min by firm struts in foam structure.

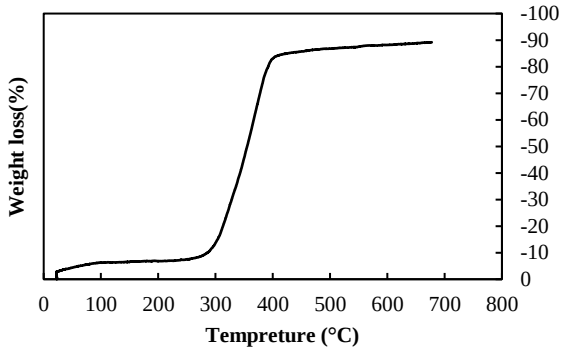

Figure 2. Thermal stability analysis of PU foam

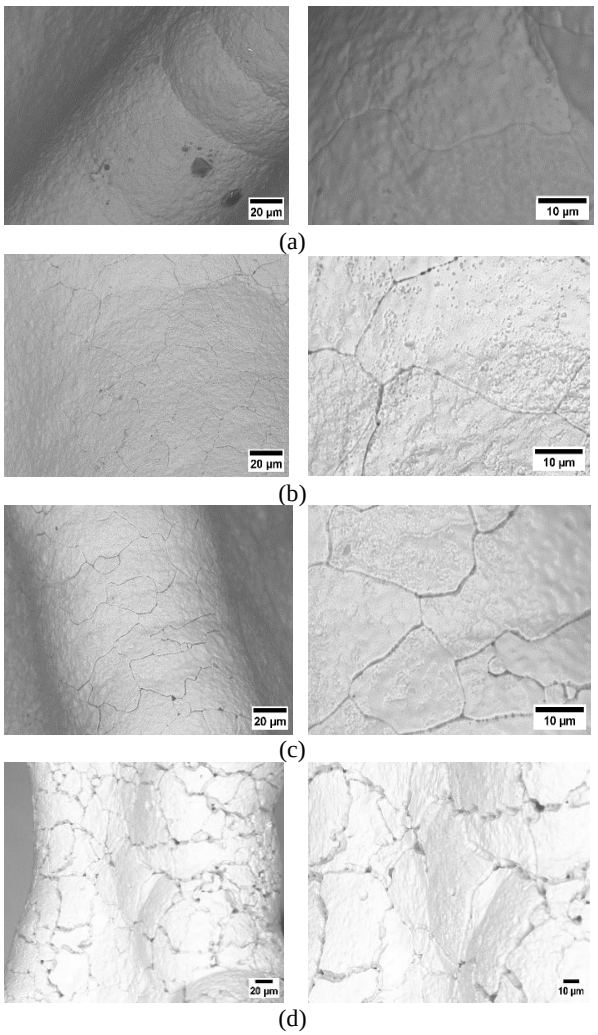

Figure 3. SEM images of surface of struts of (a) pure nickel foam, (b) pretreated nickel foam at 70 ºC for 10 min, (c) pretreated nickel foam at 80 ºC for 10 min, and (d) pretreated nickel foam at 80 ºC for 15 min

According to XRD patterns illustrated in Figure 4, three primary reflections at 2θ of 44.64°, 51.92°, and 76.46° designated to the (111), (200), and (220) planes of the face-centered-cubic (FCC) nickel, confirmed that Ni was the dominant constituent of the obtained foam (JCPDS no. 04-0850). Meanwhile, there were small peaks of Ni-P in the XRD pattern, due to the sodium hypophosphite reducing agent in the plating solution. However, by reducing the concentration of the reducing agents and plating solution with a higher pH, the amount of phosphorus and sodium to form the Ni-P layer can be minimized [16]. For nickel foam coated by Ni-γ-alumina in this study displayed spinel $NiAl_2O_4$ at 2θ=31.4°, 45°, 68.9°, 80° (JCPDS no. 10-0339). However, some other detected peaks 2θ= 25.1°, 37.7°, 57.5°, 68°, and 70° corresponding to deposited alumina (JCPDS no. 46-1212) and rhombohedral phase NiO at 2θ= 43°, 62.8° (JCPDS no. 22-118) was observed and via the following reaction and calcination at temperatures above 700 ºC, the $NiAl_2O_4$ formed as Equation (5). Calcination causes formation of $NiAl_2O_4$ spinel phase, especially in the case of Al_2O_3 (γ) presence [47].

$$NiO + Al_2O_3 = NiAl_2O_4 \quad (5)$$

Here, surface area of Ni-alumina(γ) foam measured by BET method and reported in Table 1 for comparison. Figure 5 indicated cross-sectional micrographs of nickel-γ-alumina nanocomposite foams. In fact, the wall thickness of 2-5 µm gained after electroless then increased to 50-80 µm by electrodeposition. In continue, by pulse electro- codeposition coating of nickel-γ-alumina nanocomposite over the former foam gave a three-dimensional structure with 230 µm thick and hollow struts. The white sections indicated foam cell struts and the grey section for the empty space between

TABLE 1. Specific surface area (BET) of investigated nickel foam catalysts

Sample	S.S.A (m^2g^{-1})	PPI
Nickel foam	1.48	45
Ni- alumina(γ) foam	48	45
Ru/Ce/Ni foam (Ni foam via CeO_2 electroprecipitation and impregnation with Ru [18]	39	75
AlSB/Ni foam aluminium tri-sec butylate (AlSB) [34]	5.6	-
AlIp/Ni foam ,aluminium isopropoxide (AlIP) [34]	6.9	-
Pre-treated Ni foam in catalytic methane decomposition (CMD) [32]	5.4	110
Pre-treated Ni foam with grown carbon nanofibers in catalytic methane decomposition(CMD) [32]	8.7	110

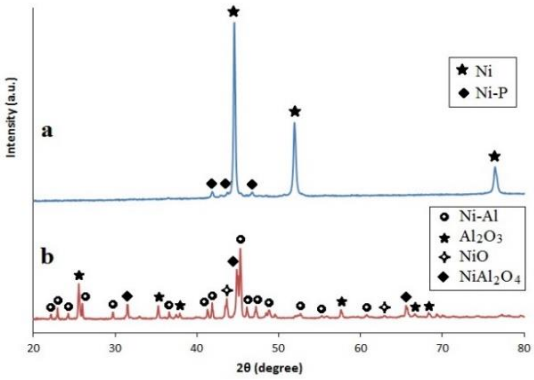

Figure 1. XRD patterns for (a) pure nickel foam and (b) nickel foam coated with nickel-γ-alumina

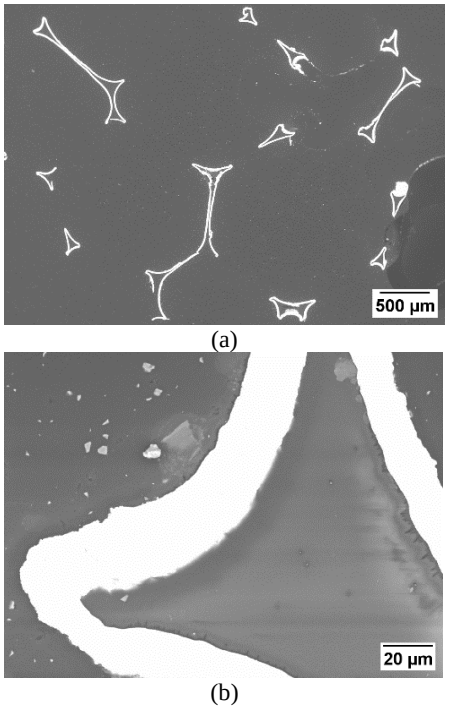

(a)

(b)

Figure 2. Optic microscopic images of electrodeposited Ni-alumina (γ) nanocomposite open cell foam specimen mounted in epoxy resin and polished, a) x40, b) x1k

the cells and the separate islands seen because of three-dimensional porous skeleton of foam appear in the surface by polishing. In the current work, using pulse codeposition of Ni/alumina(γ) reinforced nanoparticles on nickel foam increased hardness from 145 to 547 (HV). The average of five different measurements determined the final hardness shown in Figure 6.

The compressive stress-strain curves of nickel foams and Ni-alumina(γ) coated foam indicated in Figure 7. In these curves, three distinct regions seen as: (i) the linear elastic deformation (cell edges yield in bending area), (ii) collapse plateau (sudden decrease in stress after the first

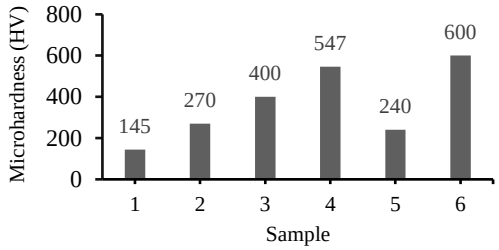

1 Nickel foam (electrodeposited Ni foam)
2 Ni coating over steel substrate [37]
3 Nickel foam (electrolyt jet electrodeposited Ni foam) [25]
4 Ni-nano γalumina codeposition over Ni foam
5 Open cell Ni−35Cr−22Fe foam(gas-phase codeposition of Cr and Fe over Ni foam) [48]
6 Ni-8.5%nano Al_2O_3 coating over steel substrate [37]

Figure 6. Results of the micro-hardness tests conducted at room temperature

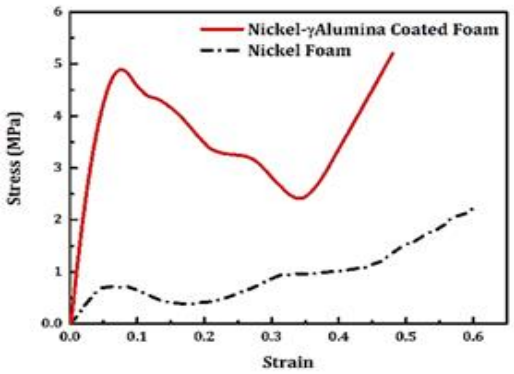

Figure 7. Compressive stress-strain curves of nickel foams and Ni-alumina(γ) coated foam

peak of stress and plateau area), and (iii) densification region (slight increase in strain, rapid growth of stress, and more significant line slope). The mechanism of linear elasticity depends on whether the cells are open or closed. At low relative densities, open-cell foams deform primarily by cell-wall bending [49, 50]. Therefore, in this study we tried to increase the strength by struts thickness growth from 50 µm to 230 µm. As shown in Figure 7, nickel foam does not oscillate from beginning to end in stage II with good compressive stability; in contrast, in the Ni-alumina(γ) nanocomposite, noticeable oscillation and a sudden decrease in stress were seen in stage II. Compressive strength (stress peak after linear elastic phase) of foams for nickel foam obtained 1.1 MPa. However, compression strength of Ni-alumina(γ) nanocomposite foam increased to 5MPa by adding reinforcement alumina nanoparticles. Ni-Al_2O_3(γ) foam compression strength increased drastically by pulse electro codeposition of the Ni-alumina and its elastic modulus improved. Reasons for increasing the strength and elastic modulus of nickel foam with the electrochemical coating are alumina nano particles. Higher compression strength could mean high mechanical stability of bottom-bed catalysts against upper-bed catalysts in the reformer where a suitable gas permeability is required. Thermal conductivity of Ni-Al_2O_3(γ) foam with density (ρ) of 0.20 gcm^{-3} calculated by measurements of thermal diffusivity (α) and specific heat capacity Cp. Thermal diffusivity (α) gained 4.41×10^{-6} m^2s^{-1} with flash xenon technique and values of specific heat capacity, Cp, measured by differential scanning calorimetry (DSC). Moreover, the changes of α by temperature rise was negligible.

The thermal conductivity calculated by Equation (6) [51, 52].

$$\lambda = \alpha \times \rho \times C_p \quad (6)$$

As stated in Table 2 by temperature rise, both Cp and thermal conductivity (λ) of nanocomposite Ni-alumina(γ) foam increased as well. Besides, the distribution of alumina coat over nickel foam and all of the other elements dispersed uniformly as seen in Figure 8. Pure nickel crystalline coatings have a truncated pyramidal structure, i.e., a typical morphology for pure nickel electrodeposits with (111) preferred texture [53, 54]. The modifications in the surface morphologies are attributed to the change from a preferred orientation to a random-oriented electrodeposit, and the addition of Al_2O_3 particulates deteriorates the pyramidal structure [54]. Considering FESEM images in Figure 9, a large number of irregularly indicated spherical nanoparticles with sizes 45 to 89 nm of Al_2O_3 and $NiO.Al_2O_3$. In fact, the layer of nanocomposite coating was less uniform and rougher with cauliflower morphology and the surface morphology could be attributed to the change from a preferred orientation to a random-oriented electrodeposition, and the embedded alumina nano particles in nickel matrix deteriorates the pyramidal structure [54, 55]. As known the reduced metal present on the surface of the catalyst was considered active in the partial oxidation of methane. The temperature-programmed reduction (TPR) can suggest the number of species and a relative classification of energy bonds between the reducing element and its environment. Ni-alumina foam specimen with a rate of 10 ºC.min^{-1} heated up to 950 º C. The result, the H_2-TPR graph in Figure 10, exhibited two reduction peaks a sharp one at 400 ºC and a broader peak at 700-720 ºC. Ni was reduced at a relatively low temperature (lower than 450 ºC). The sharp peak at 400 ºC was related to nickel oxide reduction having weak interaction with alumina support and this reduction leads to the deposition of nickel metal on γ-Al_2O_3. In contrast, the second broader peak at 700-720 ºC

relates to the reduction of the spinel $NiAl_2O_4$ occurred at high temperature in a large range of temperatures [56, 57].

As depicted in Figure 11, the conversion of methane to products was calculated via the difference between inlet and outlet flowrates ($F_{CH4.in}$, $F_{CH4.out}$) measured by online GC. After about two hours, the conversion of CH_4 reached 44% at 500 ºC. The conversion of MSR reaction calculated by Equation (5). However, with the Boudouard reaction as Equation (4) occurrence at low temperatures (300–450 ºC) carbon deposited on catalyst's surface during MSR and caused it to deactivate some parts of the nickel foam catalyst and declined its efficiency.

For the selectivity, the below equation was used. The selectivity toward the hydrogen production calculated by Equation (6) that $F_{H2.out}$ was outlet H_2 flowrate in online GC, then, the selectivity H_2 gained 2.4 upon reaching steady state phase as shown in Figure 12. Figure 13 depicted compositions of methane and hydrogen in the outlet at different time intervals for nickel foam coated with nickel-alumina(γ). Hydrogen synchronized with methane conversion and did not change significantly after 60 min. Methane exhibited a slight decreasing behavior with time. After 90 min stream time at 500 ºC, H_2 and CH_4 reached 64.2% and 18%, respectively. The flowrate of hydrogen in the outlet did not match with stoichiometry of the reaction and there is an approximately 10 – 20 % error. This difference could be attributed to the purge of hydrogen at the beginning of the process and reduction of free NiO at lower temperature gave small metallic nickel particles.

TABLE 1. Specific heat capacity (Cp) measurement by temperature

T (◦C)	Cp ($Jg^{-1}◦C^{-1}$)	Thermal Conductivity ($Wm^{-1}◦C^{-1}$)
150	0.92	0.81
250	1.00	0.88
300	1.08	0.95
350	1.17	1.03
400	1.21	1.06
450	1.31	1.15
500	1.43	1.26
550	1.53	1.35

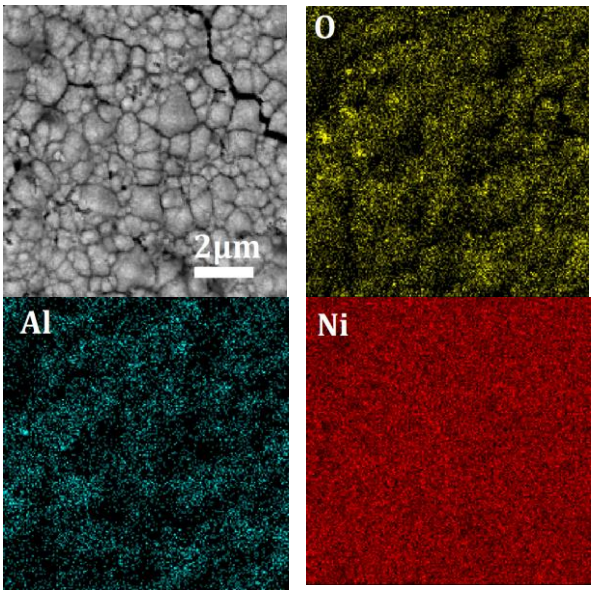

Figure 3. Map of the uniform dispersion of alumina on the Ni foam

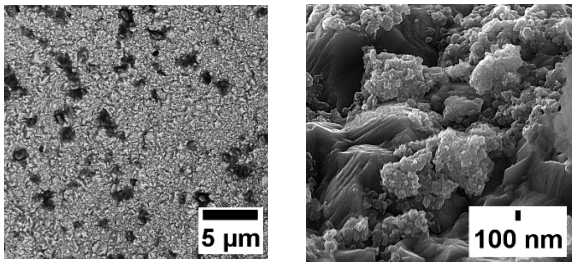

Figure 9. FESEM images of synthesized nickel foam with pulsed deposition of Ni-Al_2O_3 (γ) at f=5 Hz, θ=50%, time= 60 min

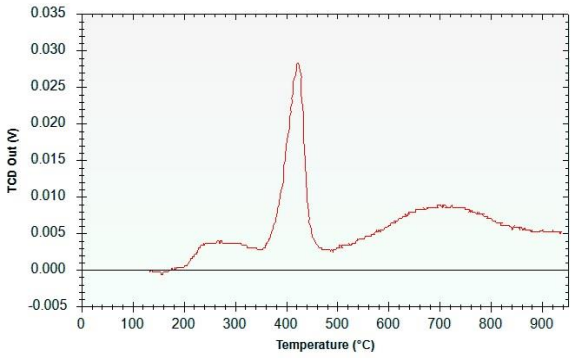

Figure 4. H_2-TPR graph of calcined nickel-alumina foam

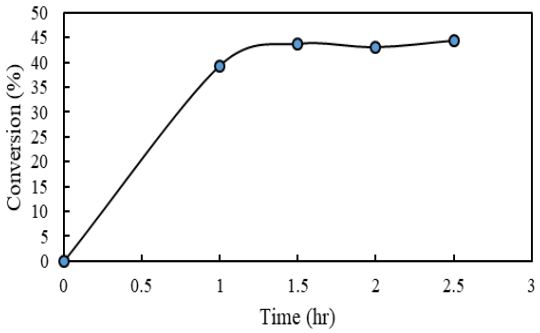

Figure 5. Methane conversion(%)-time of MSR

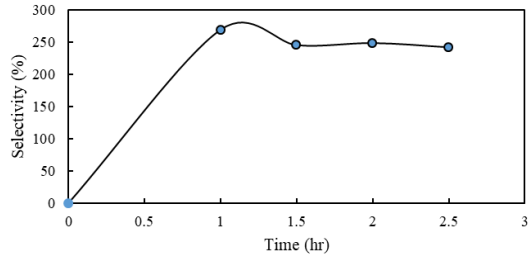

Figure 6. H_2 selectivity-time produced in MSR

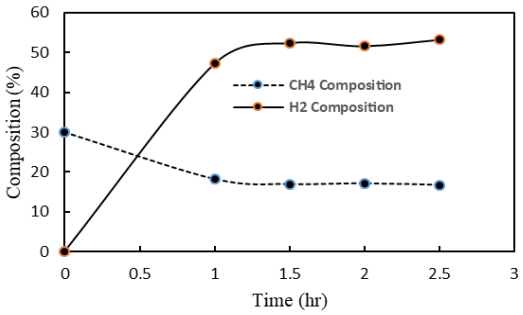

Figure 7. Composition of hydrogen and methane in the outlet of a MSR reactor

The free nickel foam without deposited alumina (metal oxide) showed no catalytic activity because the interface between nickel and alumina assumed as active sites necessary for catalytic reactions and the nickel-alumina interface by the presence of $NiAl_2O_4$ nanoparticles spinel improved catalytic properties. In nickel-γalumina foam catalysts, coating Al_2O_3(γ)nanoparticles with high specific surface area over metal foam with high thermal conductivity improve heat transfer in MSR reformers. Then, at lower temperatures, the required heat flux provided with the appropriate efficiency in MSR [9, 22]. Furthermore, the use of metal foam increases CH_4 conversion due to improved heat distribution inside the reformer with better contact between the gas mixture and the open-cell foam catalyst.

$$\text{Conversion } CH_4(\%) = \frac{(F_{CH_4 in} - F_{CH_4 out})}{F_{CH_4 in}} \times 100 \quad (7)$$

$$SH_2 = \frac{(F_{H\,2out})}{F_{CH_4.out} - F_{CH\,4.in}} \times 0.5 \quad (8)$$

To produce hydrogen, H_2O reacts with nickel surface atoms to absorb oxygen and produce gaseous hydrogen. Methane was also adsorbed on nickel surface atoms. The adsorbed methane either reacts with the adsorbed oxygen or decomposes to form chemical radicals [58].

Considering the catalytic test in this study, it resulted that the favorable temperature for the MSR decreased to 500 ºC compared to the common MSR reaction temperature at 700 ºC to 720 ºC. It could be concluded that here open-cell nickel foam coated with Ni-alumina utilization as nanocatalyst caused better heat transfer through reaction chambers and furthermore somehow the purged H_2 into the reactor for the catalysts reduction, the unreacted hydrogen can be burned to supply heat.

4. CONCLUSIONS

In this work, coating Ni-Al_2O_3(γ) nanocatalyst by pulse electrocodeposition over nickel foam is a way to enhance the thermal properties of it for MSR. Results indicated that the catalysts prepared by the nickel foam yielded higher thermal conductivity and compression strength compared to the nickel based pellet catalyst. By measuring thermal diffusivity(α) gained $4.41\times10\text{-}6$ m^2s^{-1} and values of specific heat capacity, Cp, and thermal conductivity (λ) increased by 65% with temperature increment between 150 to 550◦C in Ni-alumina(γ) foam nanocatalyst. XRD analysis indicated NiO, $NiAl_2O_4$ in the synthesized nickel-alumina(γ) foam. The nickel-alumina(γ) nanocomposite plus $NiAl_2O_4$ and alumina(γ) nanoparticles increased the hardness to 547 (HV) and the compressive strength of the fabricated nanocatalyst from 1.1 MPa to 5 MPa with a progressive crushing instead of a brittle failure. In addition, S_{BET} of the pure nickel foam was 1.48 m^2g^{-1}, which increased to 48 m^2g^{-1} by adding alumina(γ) nano particles. The Ni-alumina(γ) nanocomposite had active sites at the nickel-alumina interface and the deposited $NiAl_2O_4$ spinel, which increased the catalytic activity of the product. The reason for the low-temperature MSR in this study could be stated as the metallic nickel foam with high thermal conductivity made it a potential attraction for the novel design in this study by decreasing the favorable temperature for the MSR to 500 ºC due to highly heat transfer compared to the traditional steam reforming reaction temperature at 700 ºC.

Despite the above advances, further improvement should be focused on effective parameters such as micro and mesopores supports and utilization of different promoters like rare earth elements such as lanthanum and cerium or their oxides in synthesizing new alloyed foam nanocatalysts for hydrogen production. However, few ínvestigations have been done to the challenges of Ni-Alumina foam nanocatalysts regeneration, as well as the kinetics study of the catalytically active sites in methane reforming reactions.

5. ACKNOWLEDGEMENT

The authors are grateful Sharif University of technology, University of Toronto for general support and Research Institute of Petroleum Industry (RIPI) of assistance catalytic pilot tests.

6. DATA AVAILABILITY

The raw/processed data required to reproduce these findings cannot be shared at this time due to technical or time limitations.

7. REFERENCES

1. Acar, C. and Dincer, I., "Review and evaluation of hydrogen production options for better environment", ***Journal of Cleaner Production***, Vol. 218, (2019), 835-849. https://doi.org/10.1016/j.jclepro.2019.02.046
2. Etminan, A. and Sadrnezhaad, S., "A two step microwave-assisted coke resistant mesoporous ni-co catalyst for methane steam reforming", ***Fuel***, Vol. 317, (2022), 122411. https://doi.org/10.1016/j.fuel.2021.122411
3. Hosseini, Z., Mollazadeh Beidokhti, S., Vahdati khaki, J. and Pourabdoli, M., "Preparation of porous alumina/nano-nickel composite by gel casting and carbothermic reduction", ***International Journal of Engineering, Transactions A: Basics***, Vol. 35, No. 1, (2022), 220-227.DOI:10.5829/IJE.2022.35.01A.21
4. Tribalis, A., Panagiotou, G.D., Bourikas, K., Sygellou, L., Kennou, S., Ladas, S., Lycourghiotis, A. and Kordulis, C., "Ni catalysts supported on modified alumina for diesel steam reforming", ***Catalysts***, Vol. 6, No. 1, (2016), 11. https://doi.org/10.3390/catal6010011
5. Silva, C.K.S., Baston, E.P., Melgar, L.Z. and Bellido, J.D.A., "Ni/al2o3-la2o3 catalysts synthesized by a one-step polymerization method applied to the dry reforming of methane: Effect of precursor structures of nickel, perovskite and spinel", ***Reaction Kinetics Mechanisms and Catalysis***, Vol. 128, No. 1, (2019), 251-269. DOI:10.1007/s11144-019-01644-3
6. Naeem, M.A., Al-Fatesh, A.S., Fakeeha, A.H. and Abasaeed, A.E., "Hydrogen production from methane dry reforming over nickel-based nanocatalysts using surfactant-assisted or polyol method", ***International Journal of Hydrogen Energy***, Vol. 39, No. 30, (2014), 17009-17023. https://doi.org/10.1016/j.ijhydene.2014.08.090
7. Pashchenko, D., "Experimental investigation of reforming and flow characteristics of a steam methane reformer filled with nickel catalyst of various shapes", ***Energy Conversion and Management***, Vol. 185, (2019), 465-472. https://doi.org/10.1016/j.enconman.2019.01.103
8. Rohani, A., Allahkaram, L. and Omidvar, A., "Effect of nickel-alumina nanoparticle catalyst on the performance of methane steam reforming process", ***American Journal of Nanoscience and Nanotechnology***, Vol. 1, No. 3, (2013), 74-78. DOI:10.11648/j.nano.20130103.13
9. Meloni, E., Martino, M. and Palma, V., "A short review on ni based catalysts and related engineering issues for methane steam reforming", ***Catalysts***, Vol. 10, No. 3, (2020), 352. https://doi.org/10.3390/catal10030352
10. Baharudin, L. and Watson, M.J., "Monolithic substrate support catalyst design considerations for steam methane reforming operation", ***Reviews in Chemical Engineering***, Vol. 34, No. 4, (2018), 481-501. https://doi.org/10.1515/revce-2016-0048
11. Maleki, B., Natheghi, H., Tayebee, R., Alinezhad, H., Amiri, A., Hossieni, S.A. and Nouri, S.M.M., "Synthesis and characterization of nanorod magnetic co–fe mixed oxides and its catalytic behavior towards one-pot synthesis of polysubstituted pyridine derivatives", ***Polycyclic Aromatic Compounds***, Vol. 40, No. 3, (2020), 633-643. https://doi.org/10.1080/10406638.2018.1469519
12. Tsiotsias, A.I., Charisiou, N.D., Yentekakis, I.V. and Goula, M.A., "Bimetallic ni-based catalysts for CO_2 methanation: A review", ***Nanomaterials***, Vol. 11, No. 1, (2020), 28. https://doi.org/10.3390/nano11010028
13. Aramouni, N.A.K., Touma, J.G., Tarboush, B.A., Zeaiter, J. and Ahmad, M.N., "Catalyst design for dry reforming of methane: Analysis review", ***Renewable and Sustainable Energy Reviews***, Vol. 82, (2018), 2570-2585. https://doi.org/10.1016/j.rser.2017.09.076
14. Barzegari, F., Kazemeini, M., Farhadi, F., Rezaei, M. and Keshavarz, A., "Preparation of mesoporous nanostructure nio–mgo–sio2 catalysts for syngas production via propane steam reforming", ***International Journal of Hydrogen Energy***, Vol. 45, No. 11, (2020), 6604-6620. https://doi.org/10.1016/j.ijhydene.2020.01.007
15. Bianchi, E., Heidig, T., Visconti, C.G., Groppi, G., Freund, H. and Tronconi, E., "Heat transfer properties of metal foam supports for structured catalysts: Wall heat transfer coefficient", ***Catalysis Today***, Vol. 216, (2013), 121-134. https://doi.org/10.1016/j.cattod.2013.06.019
16. Zafardoagoo, M. and Sadrnezhaad, S.K., "Synthesis of porous nickel foam based on electroless plating on polymeric substrate and electrodeposition", ***Journal of Advanced Materials and Technologies***, Vol. 11, No. 1, (2022), 69-79. https://doi.org/10.30501/jamt.2022.325426.1210
17. Kulshreshtha, A. and Dhakad, S.K., "Preparation of metal foam by different methods: A review", ***Materials Today: Proceedings***, Vol. 26, (2020), 1784-1790. https://doi.org/10.1016/j.matpr.2020.02.375
18. Cimino, S., Cepollaro, E.M., Lisi, L., Fasolin, S., Musiani, M. and Vázquez-Gómez, L., "Ru/ce/ni metal foams as structured catalysts for the methanation of CO_2", ***Catalysts***, Vol. 11, No. 1, (2021), 13. https://doi.org/10.3390/catal11010013
19. Settar, A., Abboudi, S. and Lebaal, N., "Effect of inert metal foam matrices on hydrogen production intensification of methane steam reforming process in wall-coated reformer", ***International Journal of Hydrogen Energy***, Vol. 43, No. 27, (2018), 12386-12397. https://doi.org/10.1016/j.ijhydene.2018.04.215
20. Ashraf, M.A., Sanz, O., Montes, M. and Specchia, S., "Insights into the effect of catalyst loading on methane steam reforming and controlling regime for metallic catalytic monoliths", ***International Journal of Hydrogen Energy***, Vol. 43, No. 26, (2018), 11778-11792. https://doi.org/10.1016/j.ijhydene.2018.04.126
21. Gokon, N., Nakamura, S., Matsubara, K. and Kodama, T., "Carbonate molten-salt absorber/reformer: Heating and steam reforming performance of reactor tubes", ***Energy Procedia***, Vol. 49, (2014), 1940-1949. https://doi.org/10.1016/j.egypro.2014.03.206
22. Palma, V., Ricca, A., Martino, M. and Meloni, E., "Innovative structured catalytic systems for methane steam reforming intensification", ***Chemical Engineering and Processing-Process Intensification***, Vol. 120, (2017), 207-215. https://doi.org/10.1016/j.cep.2017.07.012
23. Basile, F., Benito, P., Del Gallo, P., Fornasari, G., Gary, D., Rosetti, V., Scavetta, E., Tonelli, D. and Vaccari, A., "Highly conductive ni steam reforming catalysts prepared by electrodeposition", ***Chemical Communications***, No. 25, (2008), 2917-2919. https://doi.org/10.1039/B801645C
24. Cheri, A. and Nebbali, R., "Numerical analysis on autothermal steam methane reforming: Effects of catalysts arrangement and metal foam insertion", ***International Journal of Hydrogen Energy***, Vol. 44, No. 39, (2019), 22455-22466. DOI:10.1016/j.ijhydene.2018.12.203

25. Chen, J., "Mechanical properties of electrolyte jet electrodeposited nickel foam", ***Journal of Engineering Science and Technology Review***, Vol. 6, No. 2, (2013), 53-56. DOI:10.25103/jestr.062.12
26. Li, Y.-g., Wei, Y.-h., Hou, L.-f., Guo, C.-l. and Yang, S.-q., "Fabrication and compressive behaviour of an aluminium foam composite", ***Journal of Alloys and Compounds***, Vol. 649, (2015), 76-81. https://doi.org/10.1016/j.jallcom.2015.07.049
27. Wang, X., Zhou, Y., Li, J. and Li, H., "Uniaxial compression mechanical properties of foam nickel/iron-epoxy interpenetrating phase composites", ***Materials***, Vol. 14, No. 13, (2021), 3523. https://doi.org/10.3390/ma14133523
28. Parveez, B., Jamal, N.A., Anuar, H., Ahmad, Y., Aabid, A. and Baig, M., "Microstructure and mechanical properties of metal foams fabricated via melt foaming and powder metallurgy technique: A review", ***Materials***, Vol. 15, No. 15, (2022). https://doi.org/10.3390/ma15155302
29. Liu, J., Zhang, L., Liu, S., Han, Z. and Dong, Z., "Effect of si content on microstructure and compressive properties of open-cell mg composite foams reinforced by in-situ mg2si compounds", ***Materials Characterization***, Vol. 159, (2020), 110045. https://doi.org/10.1016/j.matchar.2019.110045
30. Chen, J., Zhang, P., Cheng, Y. and Liu, J., "On the crushing response of the functionally graded metallic foams based on 3d voronoi model", ***Thin-Walled Structures***, Vol. 157, (2020), 107085. https://doi.org/10.1016/j.tws.2020.107085
31. Somwanshi, S.B., Somvanshi, S.B. and Kharat, P.B., "Nanocatalyst: A brief review on synthesis to applications", in Journal of Physics: Conference Series, IOP Publishing. Vol. 1644, No. 1, (2020), 012046. DOI:10.1088/1742-6596/1644/1/012046
32. Ren, Z., Zhang, J., Bai, Y., Wang, J., Chen, H., Hao, Q. and Ma, X., "Unsupported nickel catalyst prepared from nickel foam for methane decomposition and recycling the carbon deposited spent catalyst", ***International Journal of Hydrogen Energy***, Vol. 46, No. 42, (2021), 21853-21865. https://doi.org/10.1016/j.ijhydene.2021.04.026
33. Chai, R., Li, Y., Zhang, Q., Zhao, G., Liu, Y. and Lu, Y., "Monolithic ni–mox/ni-foam (m= al, zr or y) catalysts with enhanced heat/mass transfer for energy-efficient catalytic oxy-methane reforming", ***Catalysis Communications***, Vol. 70, (2015), 1-5. https://doi.org/10.1016/j.catcom.2015.07.007
34. Pegios, N., Schroer, G., Rahimi, K., Palkovits, R. and Simeonov, K., "Design of modular ni-foam based catalysts for dry reforming of methane", ***Catalysis Science & Technology***, Vol. 6, No. 16, (2016), 6372-6380. http://dx.doi.org/10.1039/C6CY00282J
35. Lajevardi, S.A., Shahrabi, T. and Szpunar, J.A., "Synthesis of functionally graded nano Al_2O_3–Ni composite coating by pulse electrodeposition", ***Applied Surface Science***, Vol. 279, (2013), 180-188. https://doi.org/10.1016/j.apsusc.2013.04.067
36. Jegan, A. and Venkatesan, R., "Characterization and optimization of pulse electrodeposition of Ni/nano- Al_2O_3 composite coatings", ***International Journal of Minerals, Metallurgy, and Materials***, Vol. 20, No. 5, (2013), 479-485. https://doi.org/10.1007/s12613-013-0754-z
37. Gül, H., Kılıç, F., Aslan, S., Alp, A. and Akbulut, H., "Characteristics of electro-co-deposited Ni– Al_2O_3 nano-particle reinforced metal matrix composite (mmc) coatings", ***Wear***, Vol. 267, No. 5-8, (2009), 976-990. https://doi.org/10.1016/j.wear.2008.12.022
38. Mirzamohammadi, S., Khorsand, H., Aliofkhazraei, M. and Shtansky, D., "Effect of carbamide concentration on electrodeposition and tribological properties of Al_2O_3 nanoparticle reinforced nickel nanocomposite coatings", ***Tribology International***, Vol. 117, (2018), 68-77. https://doi.org/10.1016/j.triboint.2017.08.003
39. Karimi, E.Z., Barzegar, F., Moloodi, A. and Zolfaghari, R., "Hardness and compressive properties of open-cell nickel foam reinforced by nano-sic particles", ***Metallurgical and Materials Transactions B-Process Metallurgy and Materials Processing Science***, Vol. 52, No. 5, (2021), 3439-3446. DOI:10.1007/s11663-021-02273-9
40. Kolaczkowski, S.T., Awdry, S., Smith, T., Thomas, D., Torkuhl, L. and Kolvenbach, R., "Potential for metal foams to act as structured catalyst supports in fixed-bed reactors", ***Catalysis Today***, Vol. 273, (2016), 221-233. https://doi.org/10.1016/j.cattod.2016.03.047
41. Syamsuir, S., Soegijono, B., Yudanto, S.D., Basori, B., Ajiriyanto, M.K., Nanto, D. and Susetyo, F.B., "Electrolyte temperature dependency of electrodeposited nickel in sulfate solution on the hardness and corrosion behaviors", ***International Journal of Engineering, Transactions C: Aspects***, Vol. 36, No. 6, (2023), 1193-1200. DOI:10.5829/ije.2023.36.06c.18
42. Oveisi, H. and Geramipour, T., "High mechanical performance alumina-reinforced aluminum nanocomposite metal foam produced by powder metallurgy: Fabrication, microstructure characterization, and mechanical properties", ***Materials Research Express***, Vol. 6, No. 12, (2020), 1250c1252.DOI:10.1088/2053-1591/ab608b
43. Kim, S., Tserengombo, B., Choi, S.H., Noh, J., Huh, S., Choi, B., Chung, H., Kim, J. and Jeong, H., "Experimental investigation of heat transfer coefficient with Al_2O_3 nanofluid chock in small diameter tubes", ***Applied Thermal Engineering***, Vol. 146, No., (2019), 346-355. DOI:10.1016/j.applthermaleng.2018.10.001
44. Sharifi, Z., Asgari, G. and Seid-Mohammadi, A., "Sonocatalytic degradation of p-chlorophenol by nanoscale zero-valent copper activated persulfate under ultrasonic irradiation in aqueous solutions", ***International Journal of Engineering, Transactions C: Aspects***, Vol. 33, No. 6, (2020), 1061-1069.DOI:10.5829/IJE.2020.33.06C.03
45. Kirgizov, A.Y., Il'yasov, I.R., Laskin, A.I. and Lamberov, A.A., "An investigation of surface transformations of nickel highly porous cellular material with an applied alumina layer during its synthesis", ***Protection of Metals and Physical Chemistry of Surfaces***, Vol. 54, No. 5, (2018), 788-794. DOI:10.1134/s2070205118040068
46. Jiao, L., Xiao, H., Wang, Q. and Sun, J., "Thermal degradation characteristics of rigid polyurethane foam and the volatile products analysis with tg-ftir-ms", ***Polymer Degradation and Stability***, Vol. 98, No. 12, (2013), 2687-2696. https://doi.org/10.1016/j.polymdegradstab.2013.09.032
47. Nikolić, V., Kamberović, Ž., Korać, M., Anđić, Z., Mihajlović, A. and Uljarević, J.B., "Nickel-based catalysts: Dependence of properties on nickel loading and modification with palladium", ***Hemijska industrija***, Vol. 70, No. 2, (2016), 137-142. DOI:10.2298/HEMIND140928090N
48. Qiu, P., WU, G.-h., SUN, D.-l., XIU, Z.-y., ZHANG, Q. and HU, Z.-l., "Compressive property and energy absorption characteristic of 3d open-cell Ni–Cr–Fe alloy foams under quasi-static conditions", ***Transactions of Nonferrous Metals Society of China***, Vol. 22, (2012), 566-572. https://doi.org/10.1016/S1003-6326(12)61762-2
49. Luo, G., Xue, P. and Li, Y.L., "Experimental investigation on the yield behavior of metal foam under shear-compression combined loading", ***Science China-Technological Sciences***, Vol. 64, No. 7, (2021), 1412-1422. DOI:10.1007/s11431-020-1786-6
50. Wan, T., Liu, Y., Zhou, C., Chen, X. and Li, Y., "Fabrication, properties, and applications of open-cell aluminum foams: A review", ***Journal of Materials Science & Technology***, Vol. 62, (2021), 11-24. https://doi.org/10.1016/j.jmst.2020.05.039
51. Mishra, R., Militky, J. and Venkataraman, M., 7 - nanoporous materials, in Nanotechnology in textiles, R. Mishra and J. Militky,

Editors. 2019, Woodhead Publishing. 311-353. https://doi.org/10.1016/B978-0-08-102609-0.00007-9

52. Speight, J.G., 3 - unconventional gas, in Natural gas (second edition), J.G. Speight, Editor. 2019, Gulf Professional Publishing: Boston. 59-98. https://doi.org/10.1016/B978-0-12-809570-6.00003-5
53. Feng, L., Ren, Y.-Y., Zhang, Y.-H., Wang, S. and Li, L., "Direct correlations among the grain size, texture, and indentation behavior of nanocrystalline nickel coatings", ***Metals***, Vol. 9, No. 2, (2019), 188. https://doi.org/10.3390/met9020188
54. Sajjadnejad, M., Omidvar, H. and Javanbakht, M., "Influence of pulse operational parameters on electrodeposition, morphology and microstructure of ni/nanodiamond composite coatings", ***International Journal of Electrochemical Science***, Vol. 12, No. 5, (2017), 3635-3651. https://doi.org/10.20964/2017.05.5
55. Shafiee, Z., Bahrololoom, M.E. and Hashemi, B., "Electrodeposition of nanocrystalline Ni/Ni– Al_2O_3 nanocomposite modulated multilayer coatings", ***Materials & Design***, Vol. 108, (2016), 19-26. https://doi.org/10.1016/j.matdes.2016.06.018
56. Tanksale, A., Beltramini, J., Dumesic, J. and Lu, G.Q., "Effect of pt and pd promoter on ni supported catalysts—a tpr/tpo/tpd and microcalorimetry study", ***Journal of Catalysis***, Vol. 258, No. 2, (2008), 366-377. https://doi.org/10.1016/j.jcat.2008.06.024
57. Daroughegi, R., Meshkani, F. and Rezaei, M., "Enhanced low-temperature activity of CO_2 methanation over ceria-promoted ni-Al_2O_3 nanocatalyst", ***Chemical Engineering Science***, Vol. 230, (2021).DOI:10.1016/j.ces.2020.116194
58. Navarro, M.V., Plou, J., Lopez, J.M., Grasa, G. and Murillo, R., "Effect of oxidation-reduction cycles on steam-methane reforming kinetics over a nickel-based catalyst", ***International Journal of Hydrogen Energy***, Vol. 44, No. 25, (2019), 12617-12627. DOI:10.1016/j.ijhydene.2018.12.056

Persian Abstract

چکیده

گرمایش بی رویه کره زمین محققین را برای ارتقاء تکنولوژی تولید انرژیهای پایدار اعم از تولید هیدروژن توسط ریفرمینگ متان–بخارآب، فرایندی اندوتررم واداشته است. در این تحقیق نانوکاتالیستی بر پایه فوم سلول باز نیکل ٤٠ (حفره در اینچ) با هدایت حرارتی بالا ساخته شد. این نانوکاتالیست با یک فرایند شیمیایی چندمرحله ای، عملیات پیش آماده سازی، تجزیه حرارتی، رسوب همنشینی الکتروشیمیایی پالسی نیکل –نانوذرات آلومینا (گاما) و کلسینه سنتز شد. ضریب دیفیوزن حرارتی(α) با تکنیک فلش زنون ٤/٤١ مترمربع بر ثانیه و ظرفیت حرارتی ویژه (Cp) توسط گرماسنجی پویشی تفاضلی(DSC) اندازه گیری شدند و محاسبه هدایت حرارتی(λ) نشان می دهد این خواص با افزایش دما از ١٥٠ به ٥٥٠ درجه سلسیوس حدود ٦٥٪فزونی می یابند. بعلاوه توسط روشهای شناسایی و آزمایشات مواد، با مقایسه فوم نیکل با فوم نیکل–آلومینا افزایش سختی از ١٤٥ به ٥٤٧ ویکرز و استحکام فشاری از ١/١ به ٥ مگاپاسکال و سطح ویژه(S_{BET})از ١/٤٨ به ٤٨ مترمربع بر گرم بدست می آید. . آنالیز پراش اشعه ایکس نشاندهنده اکسید نیکل و $NiAl_2O_4$ در ساختار می باشد. فصل مشترک بین جزء کاتالیستی$NiAl_2O_4$ و نیکل روی قابلیت کاتالیتی اثرگذاشته و کارایی این نانوکاتالیست در تست پایلوت در دمای پایین ٥٠٠ درجه سلسیوس نسبت به نتایج گزارش شده توسط تحقیقات دیگر در ٧٢٠ درجه سلسیوس یکسان بدست آمد.